

Electronic Supplementary Information

Anti-corrosive electrolyte design for extending the calendar life of lithium metal batteries

Minkwan Kim,^{‡a} Jiwoo An,^{‡a} Seung-Jae Shin,^{‡c} Insu Hwang,^a Jimin Lee,^a Youngbin Park,^a Jinyoung Kim,^a Eunseok Park,^a Jisub Kim,^a Gyuleen Park,^a Sujin Kim,^a Ali Coskun,^{*b} and Jang Wook Choi^{*a}

^a School of Chemical and Biological Engineering and Institute of Chemical Process, Seoul National University, 1 Gwanak-ro, Gwanak-gu, Seoul 08826, Republic of Korea. E-mail: jangwookchoi@snu.ac.kr

^b Department of Chemistry, University of Fribourg, Fribourg 1700, Switzerland. E-mail: ali.coskun@unifr.ch

^c Thomas Young Centre and Department of Materials, Imperial College London, London, SW7 2AZ UK

[†] Electronic Supplementary Information (ESI) available: See DOI: 10.1039/x0xx00000x

[‡] These two authors contributed equally to this work.

Experimental Section

Materials

1,2-Dimethoxyethane (DME, anhydrous, 99.5% inhibitor free) and *n*-hexane (anhydrous) were purchased from Sigma-Aldrich (USA). Lithium bis(fluorosulfonyl)imide (LiFSI, > 98%) and hexafluoro isopropyl methyl ether (HFME, > 98%) were purchased from TCI Chemicals (Japan). Li (20 μm thick on Cu foil), Cu foil, Al foil, $\text{LiNi}_{0.8}\text{Co}_{0.1}\text{Mn}_{0.1}$ (NCM811), and the polyethylene (PE) separator were purchased from Wellcos Corporation (South Korea). Super P was purchased from MTI Corporation (South Korea). *N*-methyl-2-pyrrolidone (NMP) was purchased from JUNSEI (Japan). The poly(vinylidene difluoride) (PVDF, Kynar) binder was purchased through a domestic vendor. 1,1,2,2-tetrafluoroethyl-2,2,3,3-tetrafluoropropyl ether (TTE) and bis(2,2,2-trifluoroethyl) ether (BTFE) were purchased from TCI Chemicals.

Electrochemical measurements

All electrolytes were prepared and handled in an argon-filled glovebox. 1.5M LiFSI DME-HFME(1:3) was prepared by dissolving LiFSI salt in a mixture of DME and HFME in a volume ratio of 1:3. For 1.5M LiFSI DME-HFME-Hex(1:2.1:0.9), HFME and Hex were pre-mixed in a volumetric ratio of 7:3, followed by additional mixing with DME in the designated volumetric ratio. LiFSI salt was then dissolved in the prepared solvent mixture.

All electrochemical measurements were performed by fabricating CR2032 coin cells in an argon-filled glovebox. The lithium foil electrodes used in the Li|Cu asymmetric cells and Li|Li symmetric cells were 12 mm in diameter and 300 μm in thickness, whereas those of the ultrathin lithium foil used for testing at a low N/P ratio of 1.37 were 10 mm and 20 μm , respectively. The amount of electrolyte injected into each cell was 60 μL . Before measurements, all cells were rested for 6 hours to ensure the electrodes were sufficiently infiltrated with the electrolyte. Galvanostatic, linear sweep voltammetry, and chronoamperometry scans were recorded using a battery cycler (WBCS3000, WonATech, South Korea). EIS measurements were conducted using a potentiostat (VSP, Bio-Logic, France) over the frequency range from 50 mHz to 1 MHz.

Full-cell tests were conducted using NCM811 cathodes that were fabricated using NMP-based slurry. The slurry consisting of NCM811, Super P, and PVDF binder in a weight ratio of 94:3:3

was cast onto Al foil using the doctor blade technique. The cast electrodes were dried at ambient pressure at 120 °C and then further dried overnight under vacuum at 60 °C. Next, the electrodes were compressed using a roll press to reach the density of 3 g cm⁻³. The active material of NCM811 was loaded at 15 mg cm⁻² corresponding to 3 mAh cm⁻². The cathodes were punched to circular discs with a diameter of 10 mm. All the full-cells were activated by three formation cycles at 0.2C (1C=200 mA g⁻¹) in the voltage range of 2.7–4.3 V.

Characterization of Materials

FE-SEM images were acquired using a JSM-7800F Prime instrument (JEOL, Japan). XPS results were recorded on an AXIS-His (KRATOS, U.K.). The detected XPS peak locations were calibrated with respect to the C 1s peak at 284.8 eV. ⁷Li NMR spectra were acquired with a 500 MHz Avance III 500 (Bruker, USA) using 1M LiCl in D₂O as an internal standard in a coaxial NMR tube. The Raman spectra of various electrolytes were obtained using a DXR2xi Raman spectrometer (Thermo Fisher, USA) with a 785 nm laser. The ionic conductivities of individual electrolytes were measured at 25 °C with an InLab 710 (METTLER TOLEDO, USA). FE-SEM, Raman spectroscopy, and ⁷Li NMR spectroscopy measurements were conducted at the National Centre for Inter-university Research Facilities (NCIRF) at Seoul National University. Cryo-TEM images were acquired with a Talos L120C (FEI company, Czech Rep.) at Seoul National University National Instrumentation Center for Environmental Management (SNU NICEM). Unless specifically mentioned otherwise, all samples used for cryo-TEM analysis were analyzed in a fully dried state. Density functional theory (DFT) calculations were performed using the Gaussian 09 software package.¹ Geometry optimizations and molecular orbital calculations were performed without restriction of symmetry, and the B3LYP hybrid density functional and the 6-311G++ (d, p) basis sets were used. This work was supported by the Korea Institute of Science and Technology Information (KISTI). We performed NpT ensemble MD simulations at 300 K and 1 bar using the Nosé-Hoover thermostat and barostat by^{2,3} using LAMMPS code.⁴ All the organic electrolyte molecules are modelled using OPLS-AA force field.⁵ Li⁺ is modelled using previously developed force field.⁶ A concentration of 1.5 M is achieved by putting 46 number of LiFSI ions in the simulation cell along with an appropriate number of solvent molecules.

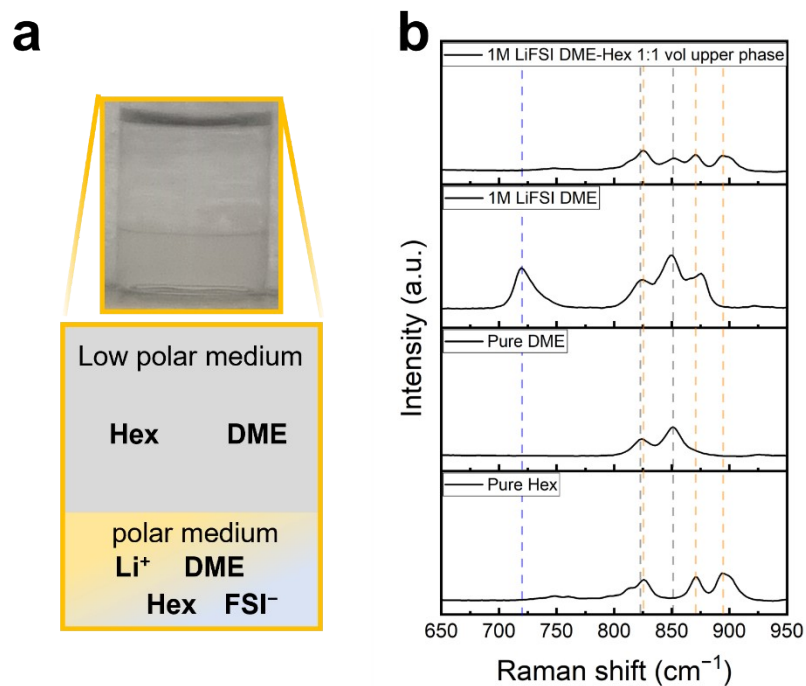


Fig. S1 Miscibility test of the electrolytes with different solvents (a) Digital photograph of 1M LiFSI in DME and *n*-hexane in 1:1 volume ratio (top) and the compositions of the separated phases. (b) Raman spectrum of the upper phase of 1M LiFSI DME-Hex 1:1 along with those of 1M LiFSI DME, pure DME, and pure Hex. Note free FSI is not detected in the upper phase.

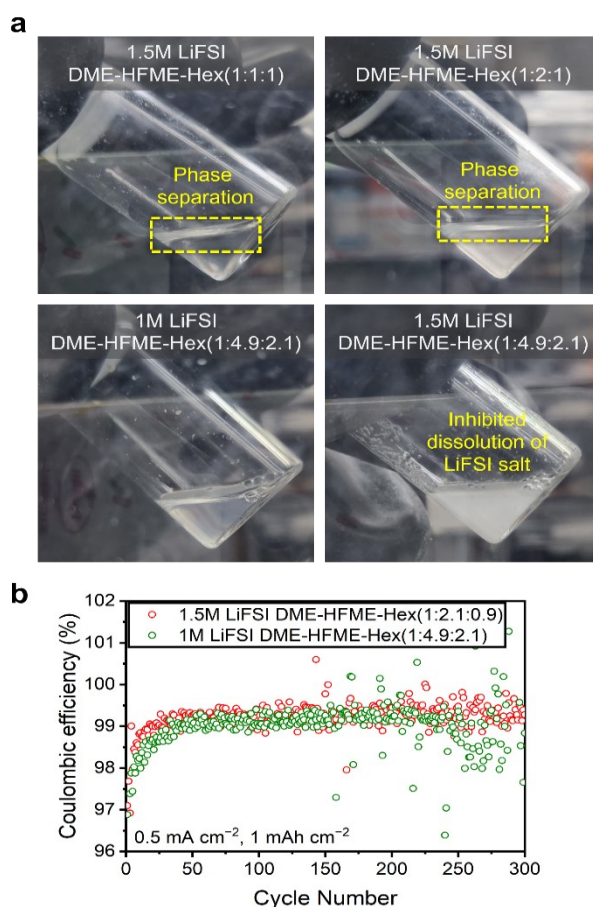


Fig. S2 Exploration of electrolyte composition. (a) Optical images of electrolytes with different compositions. (b) Comparison of cycling performance of Li|Cu asymmetric cells.

In our electrolyte blend design, one primary goal was to incorporate as much of the inexpensive and inert Hex as possible without phase separation. However, the ratio of 1:1:1 and 1:2:1 all induced the phase separation. A slight adjustment in the ratio to 1:2.1:0.9 successfully homogenized the electrolyte without inducing phase separation. While further adjustment was possible (i.e., increasing the portion of HFME and decreasing the portion of Hex from this point), such modifications would deviate from our initial design principle of maximizing Hex content. Alternatively, we investigated a novel ratio, 1:4.9:2.1, which maintains an equal ratio between HFME and Hex compared to the 2.1:0.9 composition. However, the substantially reduced DME portion in this ratio hindered the dissolution of the 1.5M LiFSI salt. Although 1M LiFSI was soluble in the 1:4.9:2.1 composition, the electrochemical performance of 1M LiFSI DME-HFME-Hex(1:4.9:2.1) was not as good as that of 1.5M LiFSI DME-HFME-Hex(1:2.1:0.9). Hence, we selected the 1.5M LiFSI DME-HFME-Hex(1:2.1:0.9) electrolyte as the optimum composition.

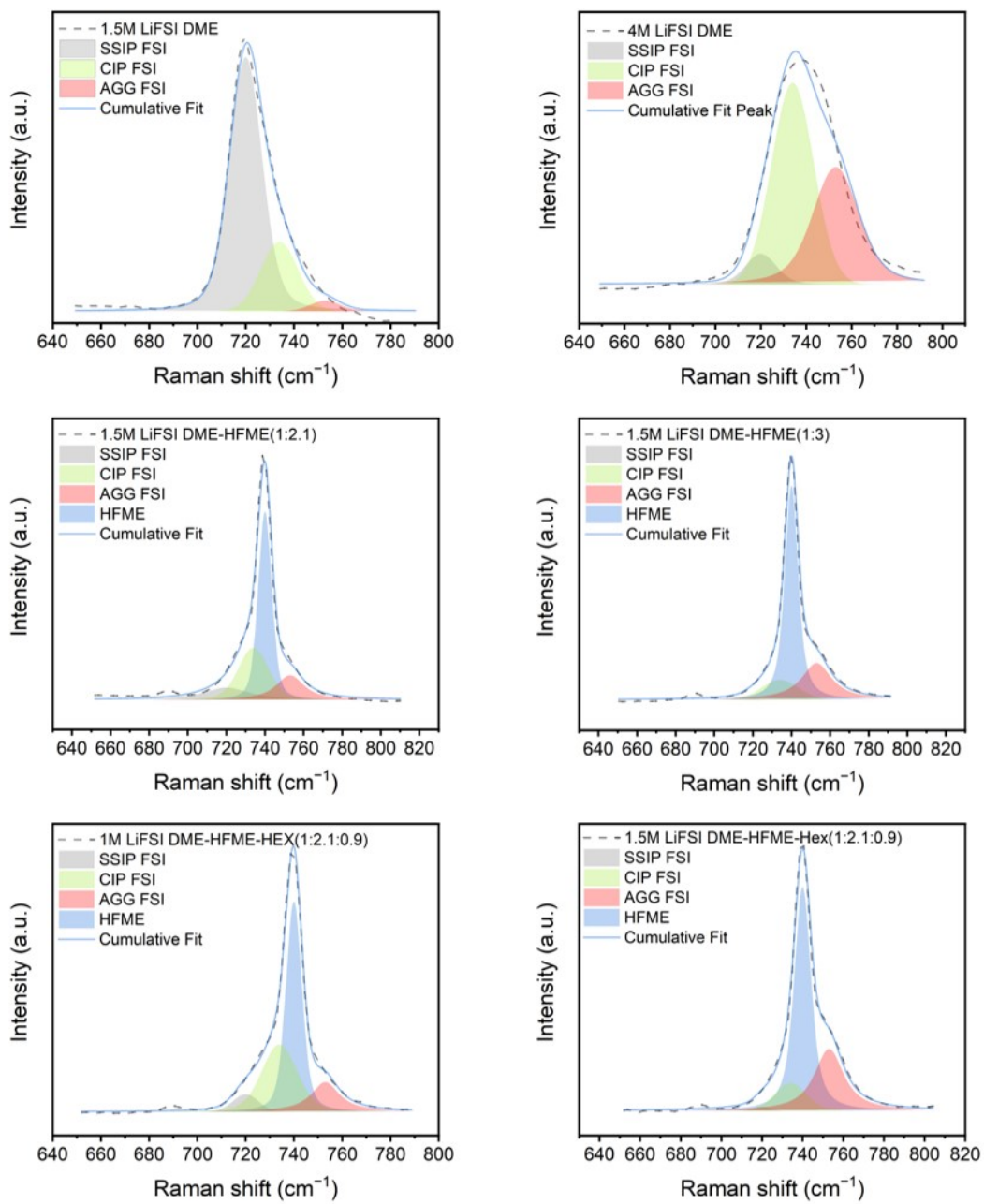


Fig. S3 Deconvoluted Raman spectra of electrolytes.

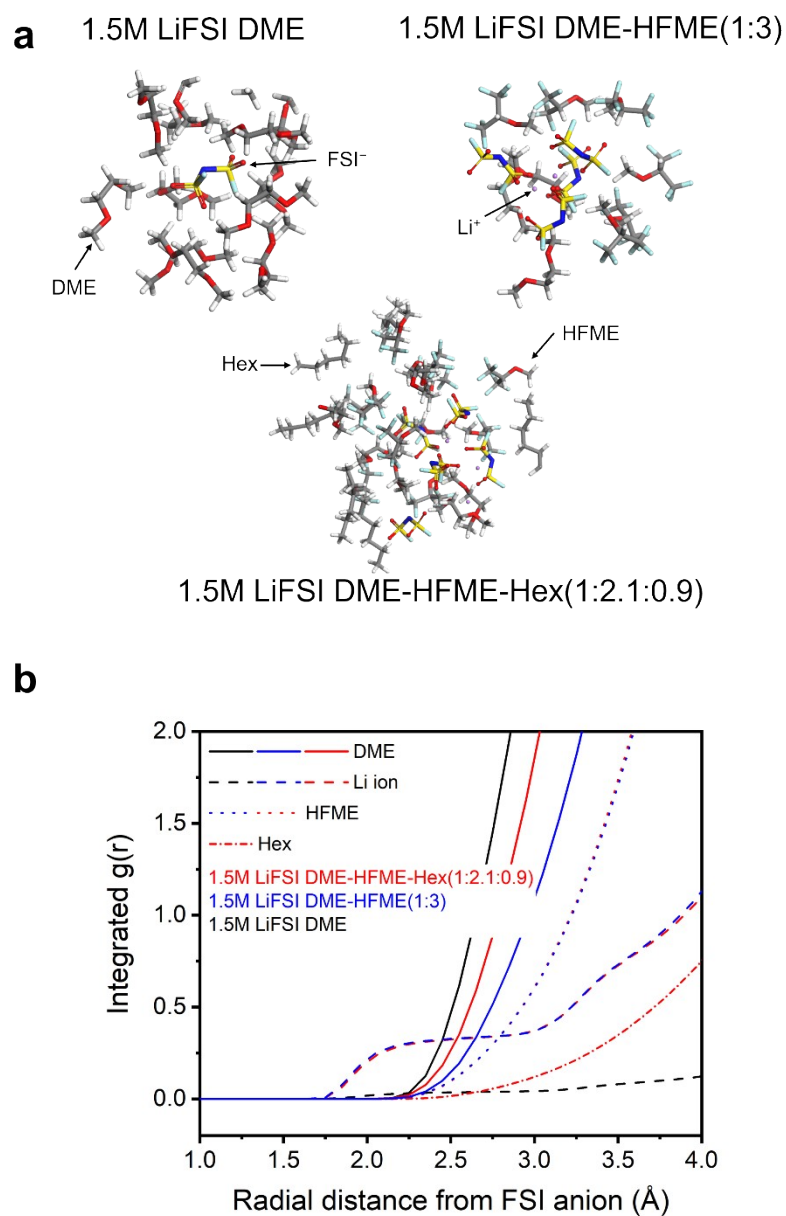


Fig. S4 Radial distances of the components in different electrolytes through MD simulations. (a) Optimized solvation structures. (b) Integrated pair distribution function $g(r)$ with respect to radial distances of molecules from FSI anion.

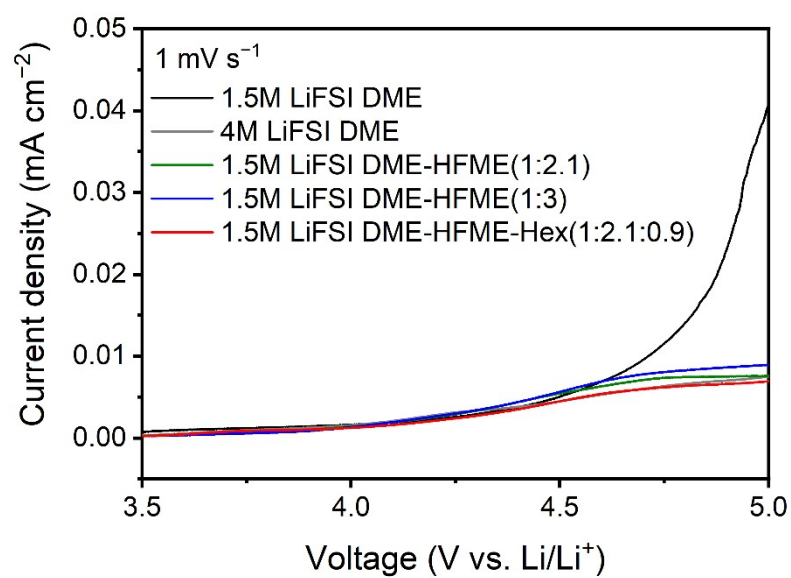


Fig. S5 Linear sweep voltammetry (LSV) analysis of the Li|Al asymmetric cells to assess the oxidative stability of electrolytes. The scan rate is 1 mV s⁻¹.

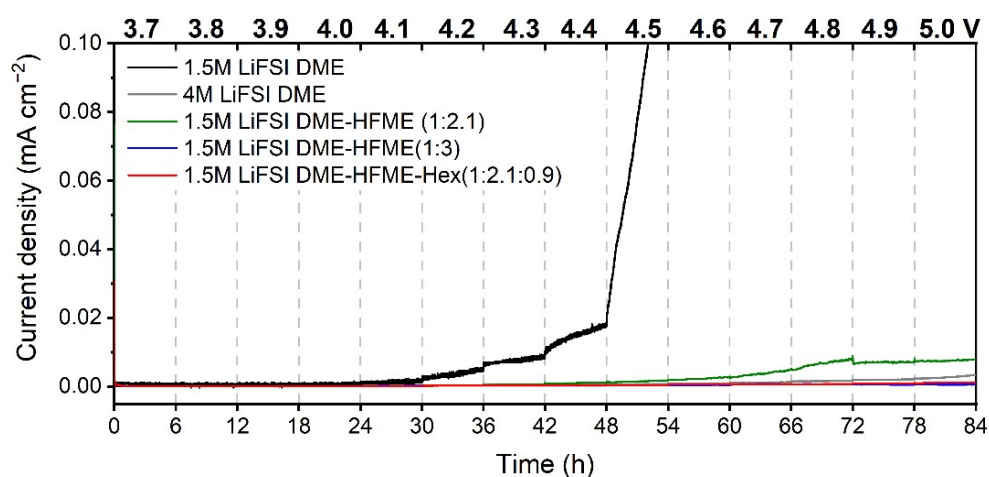


Fig. S6 Stepped chronoamperometry (CA) analysis of the Li|Al asymmetric cells. Each step was potentiostatically held for 6 hours. The voltage was increased stepwise from 3.7 V to 5.0 V in intervals of 0.1 V. Before evaluating the reversibility of Li plating/stripping with the different electrolytes, we assessed the oxidative stability of 1.5M LiFSI DME-HFME(1:2.1) with a significantly large fraction of CIP. The linear sweep voltammetry (LSV) test seemed to suggest that this electrolyte is stable at high voltage up to 5 V (vs. Li/Li⁺) (Fig. S5). Nonetheless, when subjected to chronoamperometry (CA) (Fig. 2d) and stepped CA tests at high voltages, 1.5M LiFSI DME-HFME(1:2.1) experienced severe oxidative destabilization originating from the anodic dissolution of the Al current collector, contrary to 1.5M LiFSI DME-HFME-Hex(1:2.1:0.9) and 1.5M LiFSI DME-HFME(1:3).

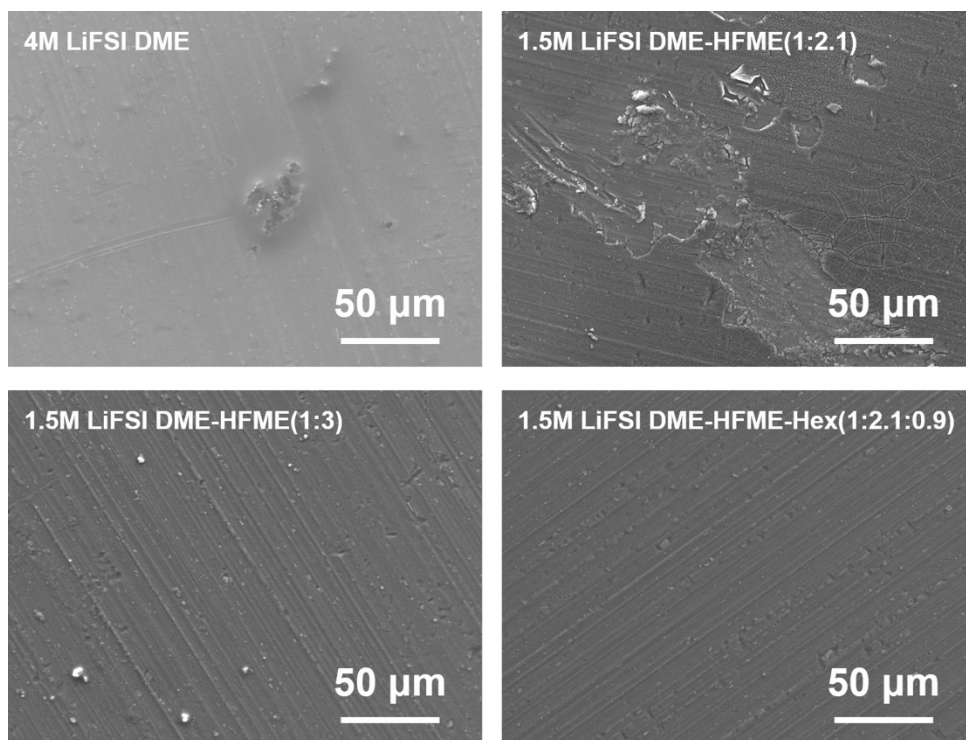


Fig. S7 SEM images of Al current collectors after CA analysis in Fig. 2d. The CA tests were conducted potentiostatically by holding the current collectors at 4.3 V (vs. Li^+/Li) for 72 hours.

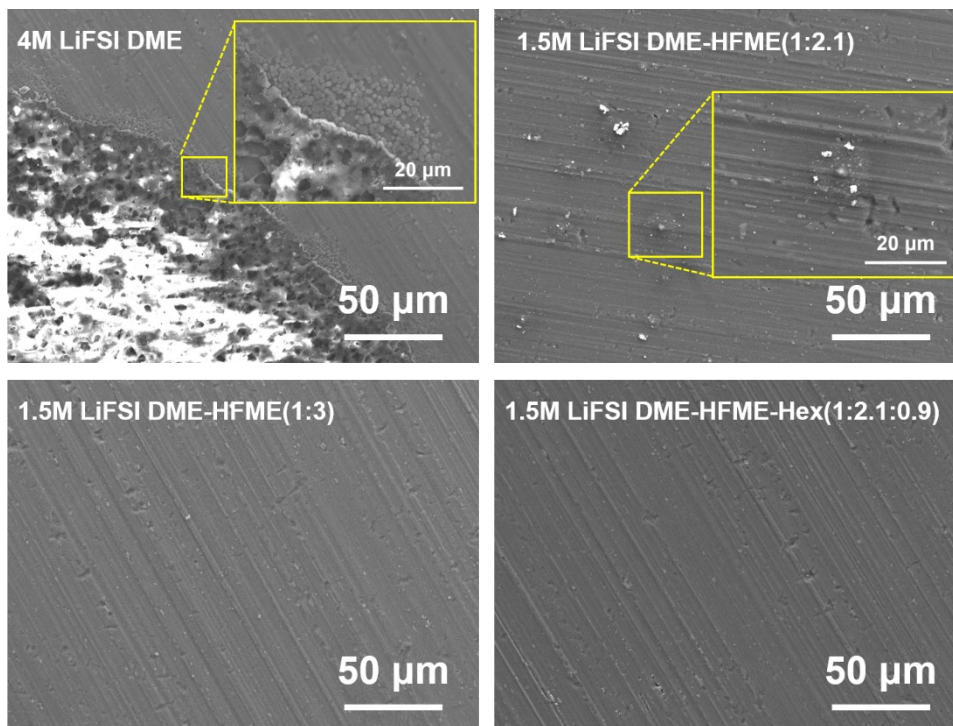


Fig. S8 SEM images of Al current collectors after the stepped CA tests in Fig. S6.

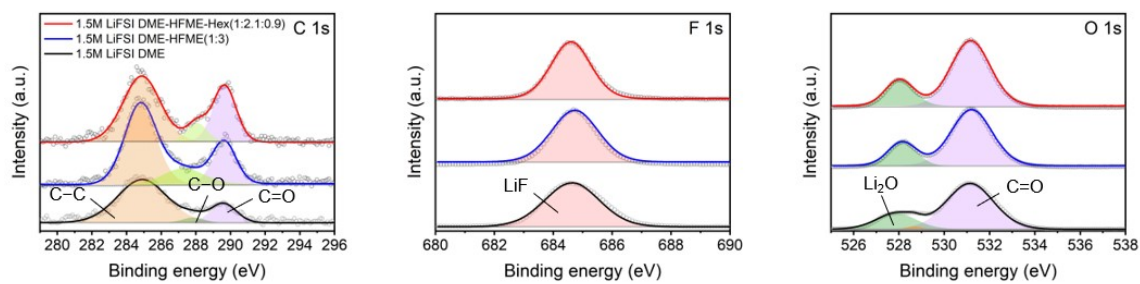


Fig. S9 XPS profiles of the SEI after 200 cycles at 1 mA cm^{-2} with a deposition capacity of 1 mAh cm^{-2} . Compared to the SEI after 5 cycles (Fig. 3d) that exhibits variations between the samples, the SEI appears to converge into a similar structure after 200 cycles.

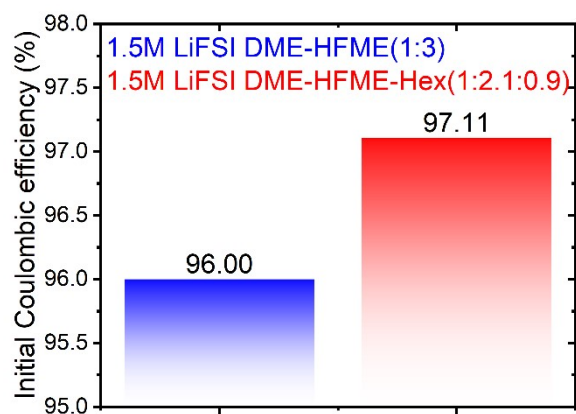


Fig. S10 Initial Coulombic efficiencies (ICEs) of the Li|Cu asymmetric cells at 1 mA cm⁻² with a deposition capacity of 1 mAh cm⁻². After the deposition, stripping was conducted at a current density of 1 mA cm⁻² until the potential reached the cutoff voltage of 1 V (vs. Li/Li⁺).

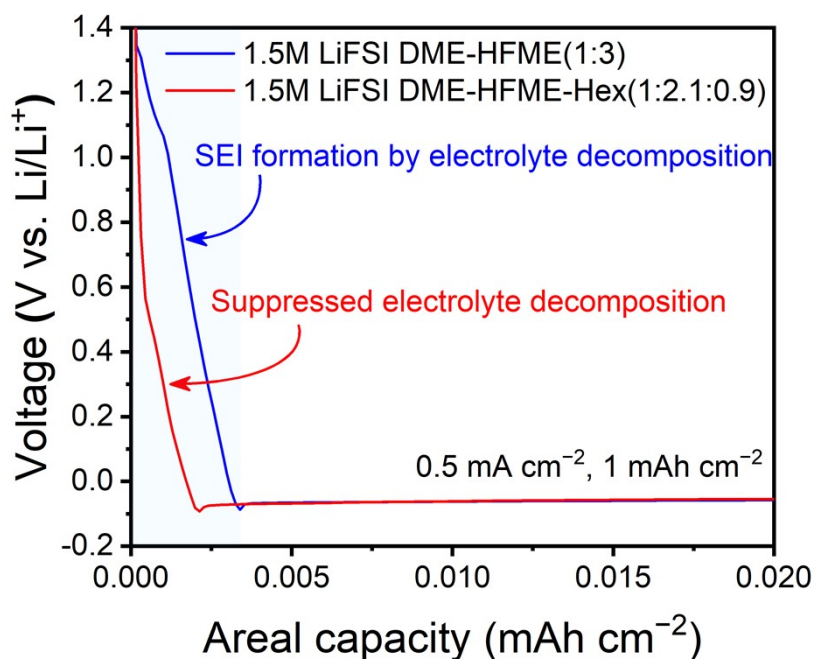


Fig. S11 Initial voltage profiles of the Li|Cu asymmetric cells in Fig. 3a. Note that capacities above 0 V (vs. Li⁺/Li) reflect the electrolyte decomposition. In 1.5M LiFSI DME-HFME-Hex(1:2.1:0.9), the negligible capacity in the range from 1.4 V to 0.6 V indicates the suppression of the electrolyte decomposition, in comparison to 1.5M LiFSI DME-HFME(1:3) that exhibited a relatively considerable capacity starting from 1.3 V.

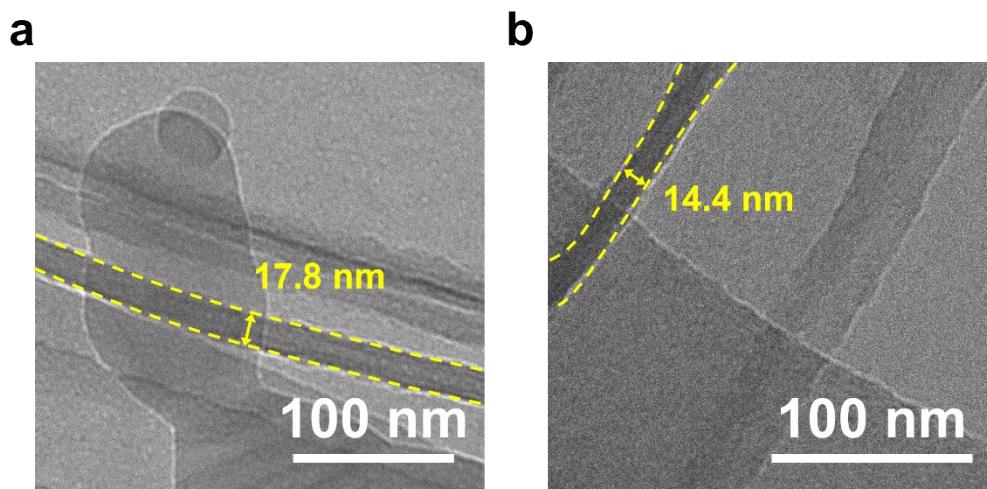


Fig. S12 Cryogenic transmission electron microscopy (Cryo-TEM) images of dried SEI. SEI on the deposited Li in (a) 1.5M LiFSI DME-HFME(1:3) and (b) 1.5M LiFSI DME-HFME-Hex(1:2.1:0.9). The deposition was conducted at 1 mA cm^{-2} with a deposition capacity of 0.1 mAh cm^{-2} on the Cu TEM grid. Note that the samples were washed with DME and dried before imaging.

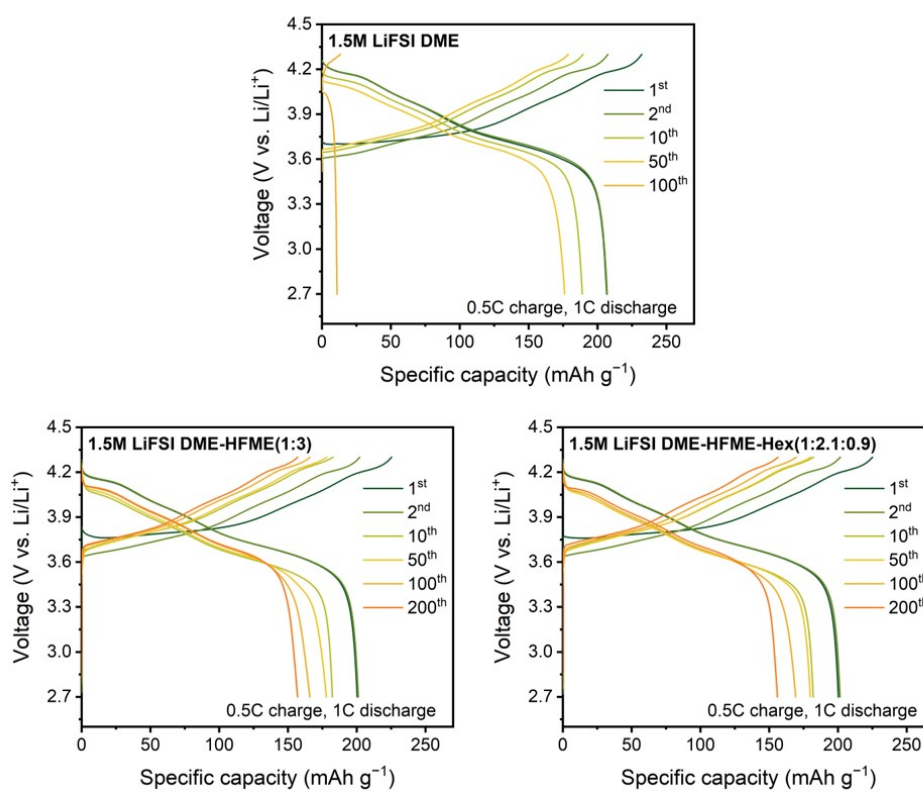


Fig. S13 Charge–discharge profiles of Li|NCM811 full-cells with various electrolytes at different cycles.

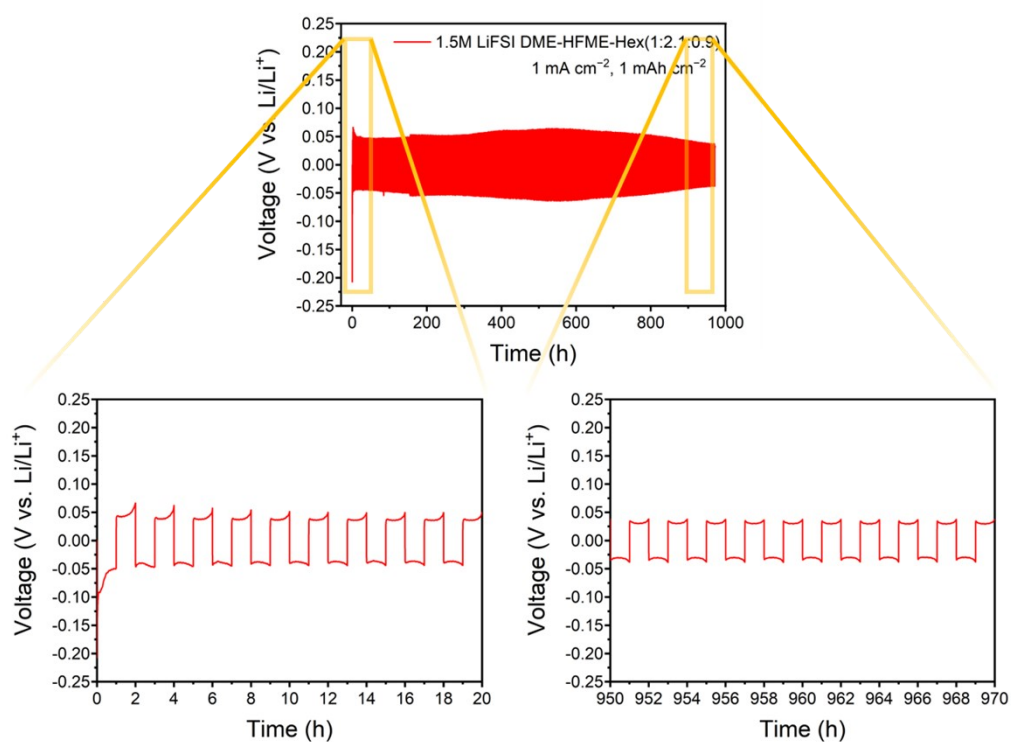


Fig. S14 Voltage-time curve of a Li|Li symmetric cell in 1.5M LiFSI DME-HFME-Hex(1:2.1:0.9) at a current density of 1 mA cm^{-2} with a deposition capacity of 1 mAh cm^{-2} .

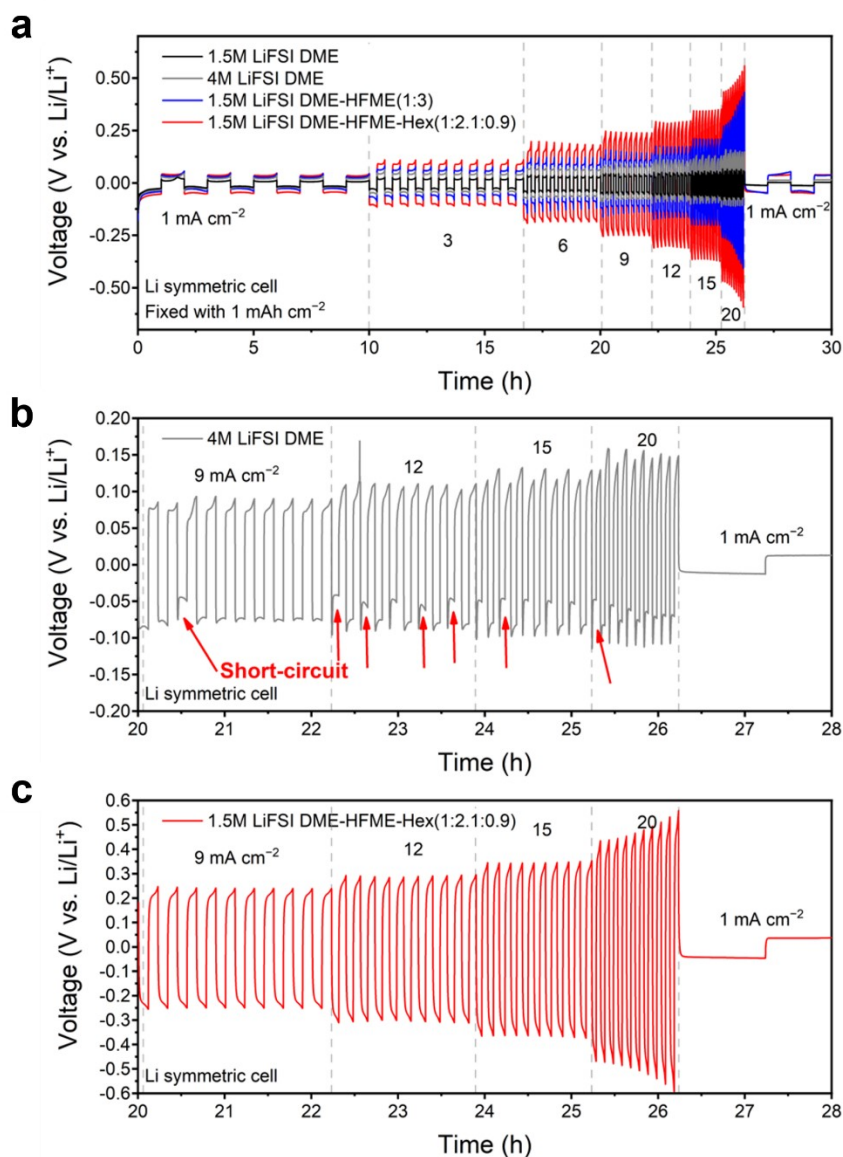


Fig. S15 Rate tests of Li|Li symmetric cells with different electrolytes. (a) Voltage profiles during rate tests with a constant capacity of 1 mAh cm⁻². **(b-c)** Magnified profiles at high current densities above 9 mA cm⁻² for **(b)** 4 M LiFSI DME and **(c)** 1.5M LiFSI DME-HFME-Hex(1:2.1:0.9).

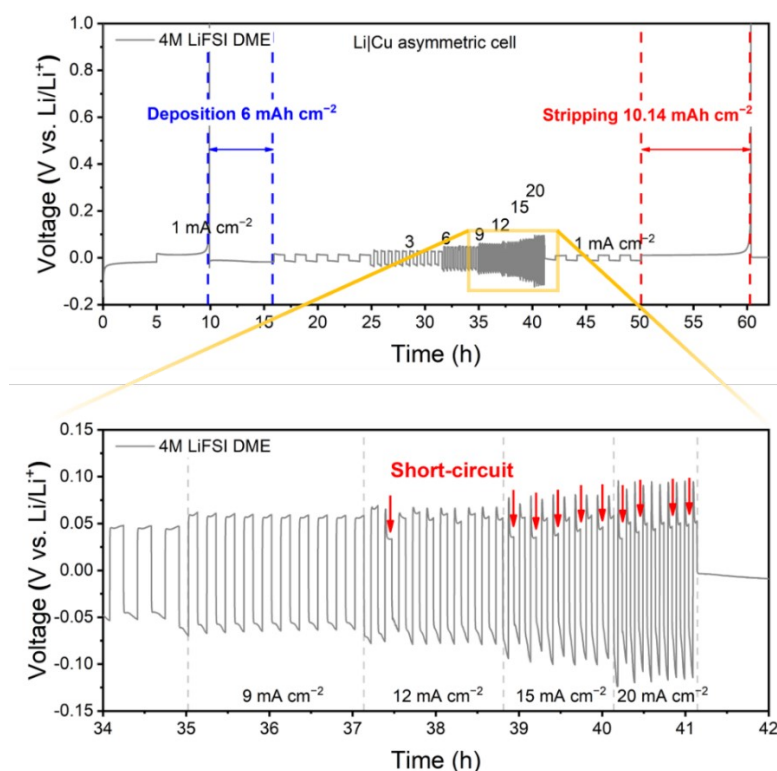


Fig. S16 Clarification of short-circuits observed in Fig. S15. The Li|Cu asymmetric cell was cycled in a modified Aurbach protocol with the same increment in the current density as in Fig. S15. After one pre-cycle of Li deposition/stripping of 5 mAh cm^{-2} at 1 mA cm^{-2} , Li of 6 mAh cm^{-2} was deposited, followed by stepwise galvanostatic cycles at different current densities as noted. During these cycles, instantaneous voltage drops were observed during Li stripping as marked with arrows (bottom figure). After the rate tests imposed with different current densities, a stripping current of 1 mA cm^{-2} was applied until the overpotential reached the cutoff voltage of 1 V (vs. Li/Li^+). The observed strip capacity of $10.14 \text{ mAh cm}^{-2}$ in this final step was much larger than the initial deposition capacity of 6 mAh cm^{-2} , implying that the current during Li stripping in the stepwise galvanostatic cycles leaked through short-circuits such that Li was accumulated on the Cu foil over repeated cycles.

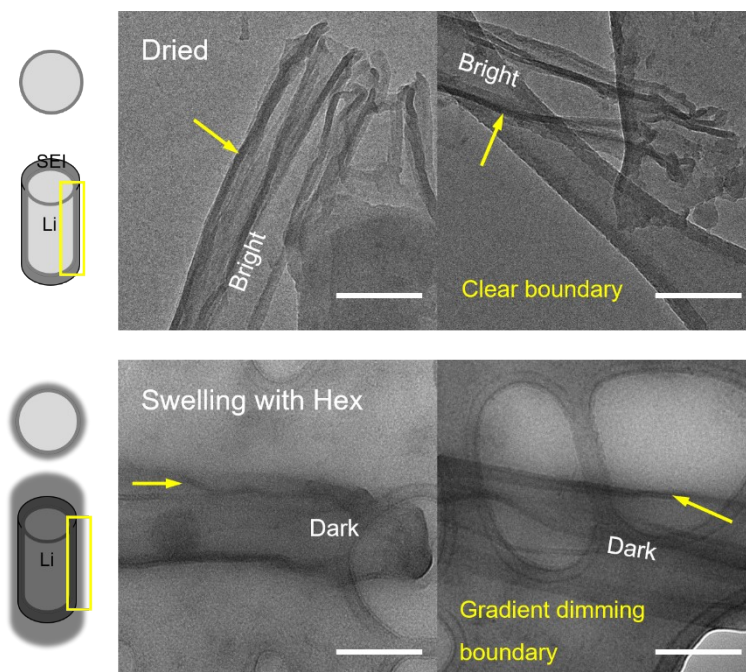


Fig. S17 Cryo-TEM images of deposited Li metal with dried and swollen samples. Li was deposited on the Cu-TEM grid with 1.5M LiFSI DME-HFME-Hex(1:2.1:0.9) at 1 mA cm^{-2} with a capacity of 0.1 mAh cm^{-2} . Dried samples (top) were imaged after rinsing the grid with DME. Swollen samples with Hex (bottom) were prepared by placing a drop of Hex on the dried samples. Note that upon adding the drop of Hex, the bright Li deposits darkened and the clear outer boundaries of the SEI faded as the SEI became swollen when penetrated by Hex. For reference, light elements (such as Li) appear bright in TEM images. The scale bars in the images are 200 nm.

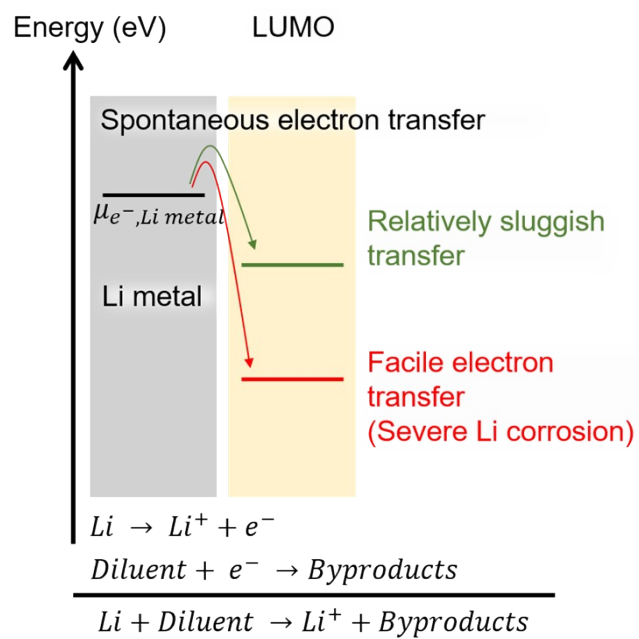


Fig. S18 Electron transfer during Li corrosion. Diluents with lower LUMO levels are more susceptible to accepting electrons, thereby accelerating Li corrosion.

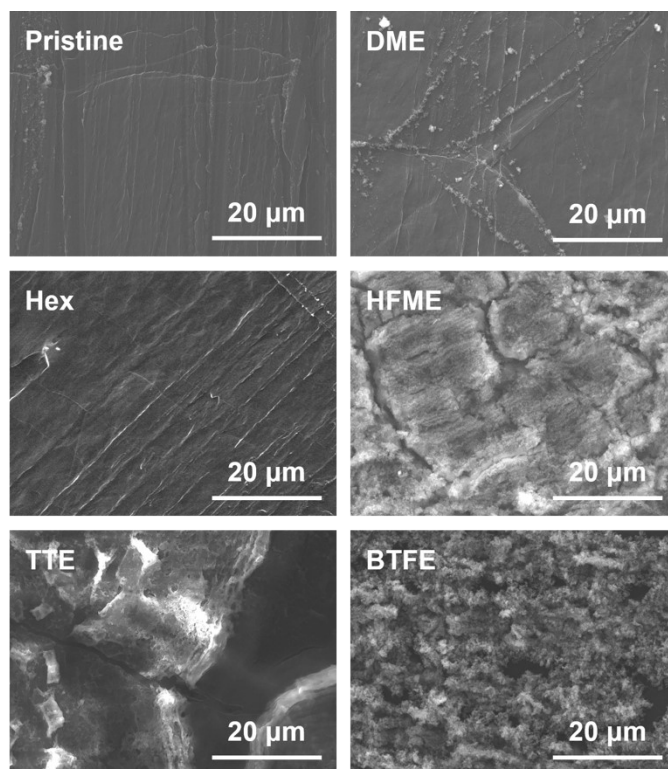


Fig. S19 SEM images of Li metal after immersion in different solvents for 24 hours. Except for DME and Hex, byproducts formed as films on the Li metal surface when immersed in HFME, 1,1,2,2-tetrafluoroethyl-2,2,3,3-tetrafluoropropyl ether (TTE), and bis(2,2,2-trifluoroethyl) ether (BTFE). This observation reflects the corrosiveness of fluorinated solvents.

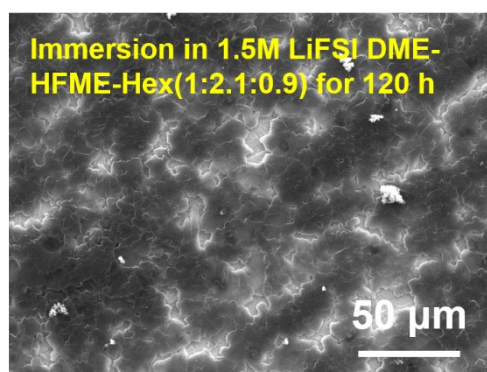
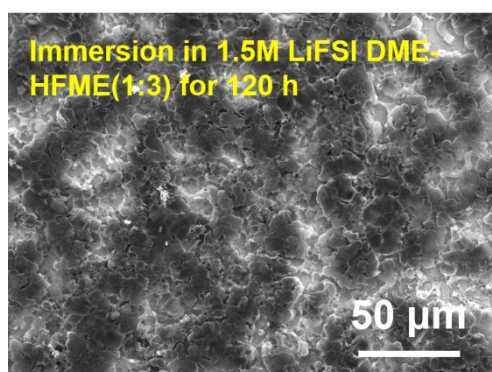
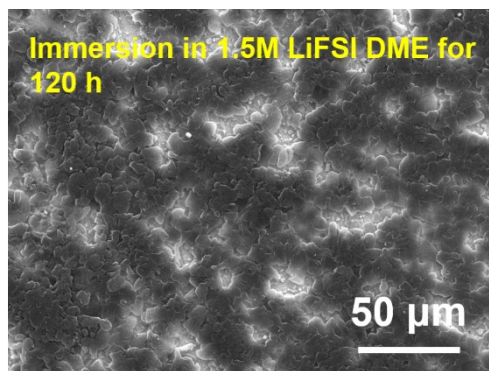


Fig. S20 Low magnification versions of the SEM images presented in Fig. 4e.

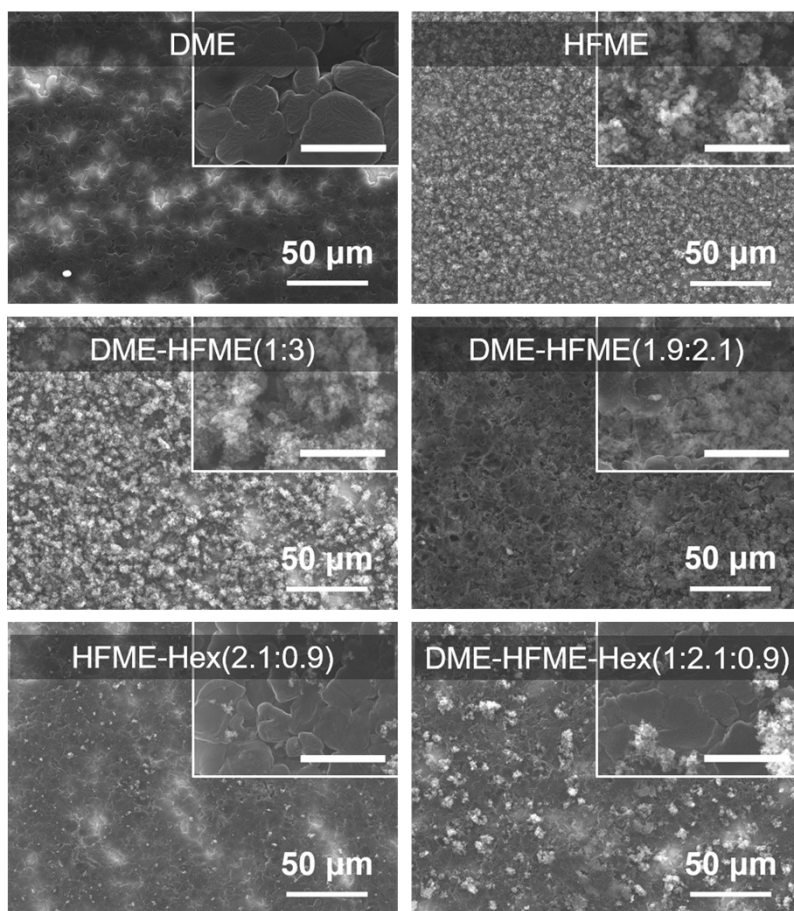


Fig. S21 SEM images of Li deposited on the Cu foil after immersion in various solvents without LiFSI salt for 120 hours. Before the immersion, Li was deposited in 1.5M LiFSI DME-HFME(1:3) (1 mAh cm^{-2} , 1 mA cm^{-2} , 5 cycles). The scale bars in the inset images are $10 \mu\text{m}$.

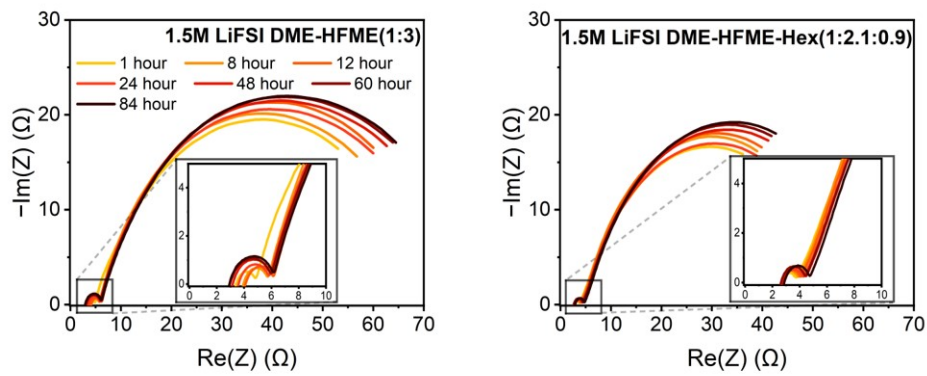


Fig. S22 Evolution of the impedances of Li|Li symmetric cells while resting with different electrolytes. After 5 cycles with a capacity of 1 mAh cm^{-2} at a current density of 1 mA cm^{-2} , EIS analysis was conducted at different points in time during a rest period of 84 h.

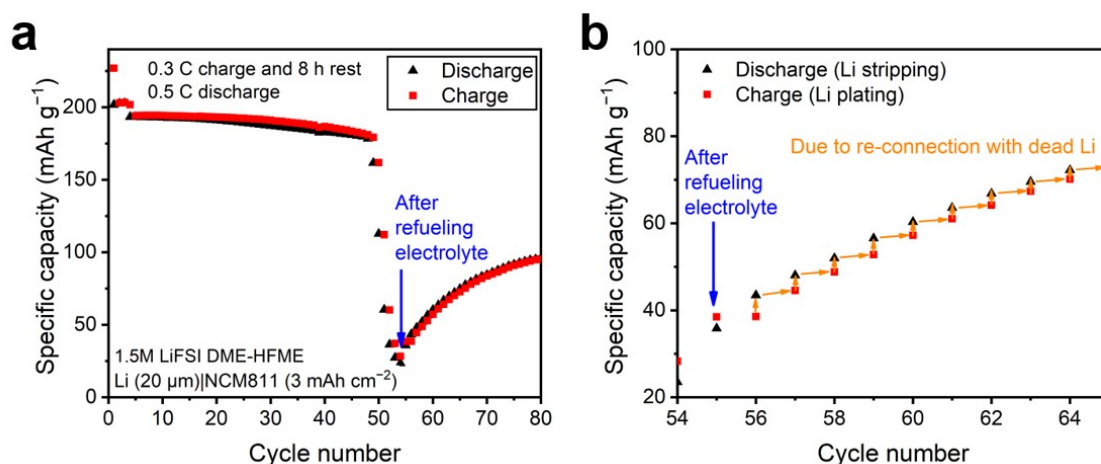


Fig. S23 Refueling test: effect on the capacity of the ceased Li|NCM811 full-cell: (a) full cycling period and (b) enlargement of the period after refueling. The same cycling conditions with rest periods as indicated in Fig. 5d–e were applied for the 1.5M LiFSI DME-HFME(1:3) full-cell. After abrupt decay at the 55th cycle, the cell was re-assembled after refueling it with 1.5M LiFSI DME-HFME(1:3). In spite of refueling with excess electrolyte and allowing sufficient time, the capacity was not fully restored. Interestingly, in specific cycles, the discharge capacities were larger than the charge capacities and were almost same as the charge capacities in the next cycles, which can be interpreted as the re-connection of newly deposited Li with dead Li. This in turn indicates that the severe formation of dead Li is responsible for the sudden capacity drop.

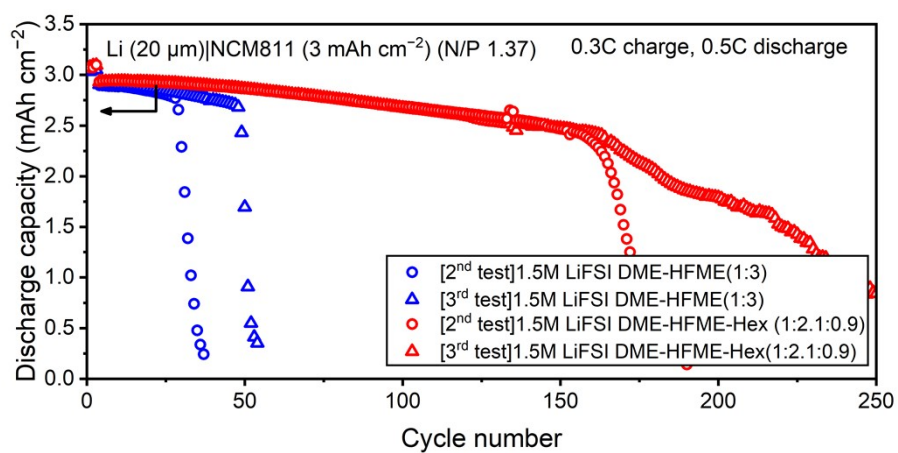


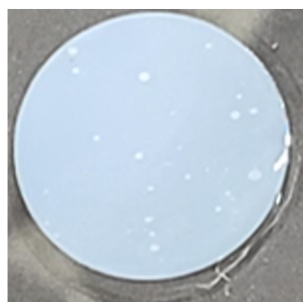
Fig. S24 Reproducibility tests of the Li|NCM811 full-cells from Fig. 5e.



1.5M LiFSI DME



4M LiFSI DME



1.5M LiFSI DME-HFME(1:3)



1.5M LiFSI DME-HME-Hex(1:2.1:0.9)

Fig. S25 Wettability tests of different electrolytes. Identical PE (polyethylene) separators were used with the same amount of electrolyte.

Table S1. Properties of hydrocarbons.

n-Hexane was selected from among a range of hydrocarbons because of its availability and appropriate viscosity at room temperature.

	Melting point (°C)	Boiling point (°C)	Viscosity (mPa·s)
Propane	-188	-42.1	
<i>n</i> -Butane	-138	-0.5	
<i>n</i> -Pentane	-129.8	36.1	0.22
<i>n</i> -Hexane	-95.3	69	0.28
<i>n</i> -Heptane	-90.6	98.4	0.389

Table S2. Properties of liquid components in the electrolytes.

The density, molecular weight (M_w), and molar volume of each liquid were considered. Because HFME has the same molar volume as Hex, replacing the HFME with the same volume of Hex does not change the total number of diluent molecules in the electrolytes.

	Density (g cm^{-3})	M_w (g mol^{-1})	Molar Volume (mol cm^{-3})
DME	0.867	90.12	0.0096
HFME	1.39	182.07	0.0076
Hex	0.655	86.18	0.0076

Table S3. Molar ratios of the components of the electrolytes.

	LiFSI	DME	HFME	Hex
1.5M LiFSI DME	1	6.09		
4M LiFSI DME	1	1.79		
1.5M LiFSI DME HFME(1:2.1)	1	1.95	3.16	
1.5M LiFSI DME HFME(1:3)	1	1.56	3.70	
1.5M LiFSI DME-HFME-Hex(1:2.1:0.9)	1	1.62	2.57	1.09

Note: HFME and Hex have the same molar volumes. Thus, the total number of diluent molecules are nearly same in 1.5M LiFSI DME-HFME(1:3) and 1.5M LiFSI DME-HFME-Hex(1:2.1:0.9).

Table S4. Densities of electrolytes.

Compared to 1.5M LiFSI DME-HFME(1:3), the 1.5M LiFSI DME-HFME-Hex(1:2.1:0.9) electrolyte contains low-density *n*-hexane instead of the same amount of high-density HFME. The low density of one electrolyte ensures that the battery system has higher energy density.

	Density (g cm ⁻³)
1.5M LiFSI DME	1.0747
4M LiFSI DME	1.4654
1.5M LiFSI DME HFME(1:3)	1.4358
1.5M LiFSI DME-HFME-Hex(1:2.1:0.9)	1.1752

References

1. W. Kohn and L.J. Sham, *Phys. Rev.*, 1965, **140**, A1133-A1138.
2. W. G. Hoover, *Phys. Rev. A*, 1985, **31**, 1695.
3. S. Nosé, *J. Chem. Phys.*, 1984, **81**, 511-519.
4. S. Plimpton, *J. Comput. Phys*, 1995, **117**, 1-19.
5. W. L. Jorgensen, D. S. Maxwell and J. Tirado-Rives, *J. Am. Chem. Soc.*, 1996, **118**, 11225-11236.
6. I. S. Joung and T. E. Cheatham III, *J. Phys. Chem. B*, 2008, **112**, 9020-9041.